

# DistributedEstimator: Distributed Training of Quantum Neural Networks via Circuit Cutting

Prabhjot Singh<sup>a,\*</sup>, Adel N. Toosi<sup>a</sup>, Rajkumar Buyya<sup>a</sup>

<sup>a</sup>Quantum Cloud Computing and Distributed Systems (qCLOUDS) Lab,  
School of Computing and Information Systems,  
The University of Melbourne, Melbourne, VIC, 3010, Australia

---

## Abstract

Circuit cutting decomposes a large quantum circuit into smaller subcircuits whose outputs are classically reconstructed to recover the original expectation values. While prior work characterises cutting overhead in terms of subcircuit counts and sampling complexity, its end-to-end impact on iterative, estimator-driven training pipelines remains insufficiently measured from a systems perspective. We propose *DistributedEstimator*, a cut-aware estimator execution pipeline that treats circuit cutting as a staged distributed workload. Each estimator query is instrumented across four phases: partitioning, subexperiment generation, parallel execution, and classical reconstruction. Using logged runtime traces and learning outcomes on two binary classification workloads (Iris and MNIST), we quantify cutting overheads, scaling limits, and sensitivity to injected stragglers, and evaluate whether accuracy and robustness are preserved under matched training budgets. Our measurements reveal that reconstruction constitutes a dominant fraction of per-query time—reaching a median of 53% and a 95th percentile of 58% at three cuts—thereby bounding achievable speed-up under increased parallelism. Despite these overheads, test accuracy is fully preserved on Iris and maintained without systematic degradation on MNIST across all evaluated cut configurations. Robustness under Gaussian noise and FGSM perturbations is similarly preserved, with several cut configurations exhibiting comparable or improved robustness relative to the uncut baseline. The exponential growth of subexperiment counts with each additional cut ( $O(9^c)$  for CNOT-based decomposition) represents a fundamental computational barrier that limits practical experimentation to small qubit counts with current methods. These results establish that practical scaling of circuit cutting for learning workloads requires reducing and overlapping reconstruction, designing scheduling policies for barrier-dominated critical paths, and developing computationally efficient reconstruction strategies for larger qubit counts.

**Keywords:** quantum neural networks, circuit cutting, distributed quantum computing, quantum machine learning, variational quantum algorithms, circuit knitting, distributed training

---

## 1. Introduction

Hybrid quantum–classical workloads are increasingly shaped by systems constraints rather than purely algorithmic ones: the circuits and training loops of practical interest frequently exceed the width, depth, or reliability envelope of near-term devices, while still requiring repeated expectation estimation in an interactive optimisation loop [1, 2, 3]. In this regime, execution is dominated by *estimator-heavy* pipelines that combine many short quantum jobs with non-trivial clas-

sical orchestration, aggregation, and optimiser feedback [4, 5]. As a result, the end-to-end performance of quantum machine learning (QML) and variational training is governed not only by circuit latency, but also by how effectively we schedule, parallelise, and reconstruct large collections of sub-tasks under heterogeneous runtimes [6, 7, 8].

Circuit cutting provides a principled mechanism to execute circuits that do not fit a target backend by decomposing them into smaller subcircuits that can be executed independently, followed by classical reconstruction of the desired quantity [9, 10, 11, 12]. This transforms a single circuit evaluation into a staged distributed workload: a fan-out of subcircuit executions, followed by a global reduction step that reconstructs the

---

\*Corresponding author.

Email address:

prabhjot.singh.1@student.unimelb.edu.au (Prabhjot Singh)

target expectation value (and, in learning settings, supports gradient estimation and optimiser updates). The methodological benefits of cutting are clear. The systems implications are less well characterised. Existing work typically reports overhead in terms of subcircuit counts, sampling complexity, or asymptotic reconstruction cost [10, 12, 13], which is informative for feasibility but does not directly answer the operational question that governs scaling: *where does wall-clock time go when we actually run the pipeline in parallel?*

### 1.1. Motivation and Problem Statement

We identify three practical limitations that motivate our study.

*P1: Overhead attribution is under-specified.* Cutting introduces additional compilation steps, subcircuit materialisation, task dispatch, and classical reconstruction. These costs are often treated as secondary to quantum execution or summarised coarsely. Without instrumentation that attributes time across stages, it is difficult to determine whether observed slowdowns are intrinsic to the cutting method or artefacts of the execution runtime and scheduling policy.

*P2: Reconstruction can dominate the critical path.* The decomposition induced by cutting increases parallelism in subcircuit execution but also concentrates work in a reconstruction stage that aggregates results across many subcircuits. In distributed computing, analogous reduction phases are known to bound scalability even when upstream work parallelises well [6, 8]. Without measuring the reconstruction share of end-to-end runtime under scale-out, it is unclear whether additional workers reduce total time or merely shift idle time upstream.

*P3: Training dynamics, accuracy, and robustness must be assessed end-to-end.* Circuit cutting aims to preserve the target computation, but in learning pipelines the optimiser observes finite-sample estimators and potentially different noise profiles. Small changes in estimator variance or evaluation ordering can alter optimisation trajectories, and practical effects may only appear when integrating cutting with training [2, 4, 3]. Moreover, if the resulting models are to be meaningful, we must check not only predictive accuracy but also robustness behaviour under the same training protocol [14, 15].

These limitations are systems problems as much as they are quantum problems: they concern staging, scheduling, aggregation, and the interaction between distributed execution and iterative optimisation.

### 1.2. Research Questions

We structure the paper around the following research questions (RQs), designed to be answered by measured runtime logs and training traces rather than by asymptotic arguments:

1. *RQ1 (Cutting overhead):* What additional end-to-end overheads are introduced by circuit cutting compared to an uncut execution baseline, and how do these overheads scale with the degree of parallelism?
2. *RQ2 (Scalability bottlenecks):* Which pipeline stages bound scaling under parallel execution, and under what conditions does classical reconstruction become the dominant contributor to wall-clock time?
3. *RQ3 (Scheduling policy and staggering):* How do execution policies that stagger or otherwise reshape subcircuit dispatch affect throughput, straggler sensitivity, and overall time-to-solution?
4. *RQ4 (Accuracy and training behaviour):* Does cutting preserve task accuracy under identical training protocols, and can the induced estimator and scheduling characteristics measurably influence training stability (e.g., convergence behaviour) relative to the uncut baseline?
5. *RQ5 (Robustness):* How does circuit cutting affect robustness metrics under the same evaluation regime, and are observed changes attributable to estimator effects rather than to changes in model definition?

We emphasise that each RQ is framed to admit an unambiguous operationalisation in our measurements: we measure stage-level durations, derive scaling trends and bottleneck shares from those measurements, and evaluate accuracy and robustness outcomes from recorded training and evaluation traces.

### 1.3. Approach Overview

To answer these questions, we design an estimator-based execution pipeline that makes cutting explicit as a staged distributed workload. At a high level, our system: (i) generates a cut plan and the associated family of subcircuits required by the chosen cutting method [10, 12], (ii) executes subcircuits as independent tasks on a distributed runtime, (iii) reconstructs target estimates via a dedicated aggregation phase, and (iv) feeds reconstructed estimates into an iterative training loop. Critically, we instrument each stage to produce time-stamped records of compilation, dispatch, execution,

and reconstruction, enabling stage-level attribution under varying degrees of parallelism and scheduling policies.

Our evaluation methodology is correspondingly systems-driven. We do not assume that more parallel workers yield proportional speed-ups; instead, we quantify where the critical path shifts as we scale out, using the same experimental protocol across baseline (no cut) and cut variants. For RQ3, we implement and compare scheduling policies that intentionally reshape concurrency (including staggering) to reduce contention and mitigate stragglers, drawing on established insights from heterogeneous cluster scheduling and tail-latency mitigation [7, 16]. For RQ4–RQ5, we couple the runtime measurements with training logs to ensure that any performance improvements are not purchased by silent degradation in model outcomes.

The pipeline is integrated with the Qiskit machine learning stack: the *EstimatorQNN* abstraction wraps the parameterised quantum circuit and observable into a differentiable neural network layer, and *TorchConnector* bridges this layer into PyTorch’s automatic differentiation and optimisation framework [17]. When circuit cutting is enabled, our *DistributedEstimator* intercepts each estimator query within this pipeline, decomposes it into subexperiments via the *qiskit-addon-cutting* library [18], dispatches them to a worker pool, reconstructs the expectation value, and returns it transparently to the *EstimatorQNN* interface. Gradients are computed via the parameter-shift rule [4], which generates additional estimator queries—each of which is independently decomposed and reconstructed through the same cut-aware pipeline. This design ensures that the training loop, loss computation, and optimiser updates remain unchanged regardless of whether cutting is enabled, isolating the systems effects of cutting from algorithmic changes to the learning procedure.

#### 1.4. Contributions

Our main contributions are as follows:

- *A measurement-driven formulation of circuit cutting as a distributed staged pipeline*, with instrumentation that attributes end-to-end time across cutting, subcircuit execution, reconstruction, and training, and with explicit integration into the QML training loop via *EstimatorQNN* and *TorchConnector*.
- *An empirical scalability analysis grounded in stage-level logs*, enabling bottleneck identification and explaining when additional parallelism does

not translate into reduced wall-clock time due to aggregation and coordination effects.

- *A study of scheduling policies for cutting workloads*, including staggered dispatch strategies, evaluated through measured throughput and tail behaviour rather than assumed ideal parallelism.
- *An end-to-end assessment of learning outcomes*, reporting accuracy and robustness under consistent training protocols to distinguish performance gains from changes in optimisation behaviour.
- *A characterisation of computational scalability barriers*, documenting the exponential growth of reconstruction overhead with cut count and establishing the computational constraints that limit practical experimentation to small qubit counts with current methods.

Together, these contributions establish a systems-level understanding of the performance trade-offs introduced by circuit cutting in estimator-heavy training pipelines, and provide a reproducible basis for reasoning about overheads, bottlenecks, and outcome preservation under distributed execution.

## 2. Background and Related Work

In this section, we summarise the technical background required to interpret our system design and measurements, and we position our work against the most relevant literature on circuit cutting, hybrid quantum–classical execution, and distributed performance bottlenecks.

### 2.1. Background

#### 2.1.1. Hybrid Quantum–Classical Workloads and Variational Training

Near-term quantum devices operate in the *Noisy Intermediate-Scale Quantum* (NISQ) regime, where limited qubit counts and noise constrain executable circuit width and depth [1]. A prevalent approach in this regime is the *variational quantum algorithm* (VQA), which couples a parameterised quantum circuit with a classical optimiser [19, 2, 20, 21]. This hybrid loop underpins much of quantum machine learning (QML), including parameterised quantum models [22, 23] and kernel-style feature maps [24]. For learning tasks with classical data, practical feasibility often depends as much on data access patterns and estimator variance as on the expressivity of the quantum model [25].

From a systems perspective, VQA training is dominated by repeated evaluation of expectation values and (often) gradients. Analytic gradient schemes such as the parameter-shift rule are attractive because they avoid finite-difference instability but still multiply circuit evaluations [4]. In addition, the optimisation landscape can be problematic (e.g., barren plateaus), which can increase the number of training iterations and amplify any per-iteration overheads [26, 2]. Consequently, end-to-end runtime is governed by a composition of quantum execution latency, the number of circuit evaluations required by the optimiser, and classical orchestration and post-processing costs [1, 2].

Noise and sampling error further complicate this picture. Error mitigation can improve estimator accuracy without full fault tolerance, but it typically adds additional circuit executions and classical processing steps [5, 3]. The resulting workload is therefore *estimator-heavy*: it comprises large numbers of small quantum jobs plus non-trivial classical aggregation, often executed in an interactive loop [3, 2].

### 2.1.2. Estimator Abstractions and Execution Models

Most near-term applications consume quantum hardware through an expectation-value interface: a circuit (or parameterised circuit) together with one or more observables yields an estimate with finite-sample variance. Modern software stacks expose this explicitly. For example, the Qiskit architecture and workflow are documented in an authoritative, citable form [27], and its *Estimator* and *Sampler* primitives formalise expectation and sampling as first-class execution units [28]. Similarly, differentiable programming toolchains integrate quantum evaluations into classical automatic differentiation and optimisation (e.g., plugin-based device backends) [29, 30].

These abstractions are convenient, but they also make performance failure modes more predictable: (i) the number of circuit evaluations grows with the estimator variance and the optimiser’s query complexity, (ii) the aggregation step becomes unavoidable for training and reconstruction, and (iii) the effective critical path may be dominated by orchestration and reduction rather than by raw quantum execution [4, 5, 3]. Our paper explicitly treats this as a distributed systems problem: we measure and attribute overheads across pipeline stages rather than assuming “quantum time” is the only knob that matters.

### 2.1.3. Circuit Cutting and Classical Reconstruction

Circuit cutting (often discussed under the umbrella of *circuit knitting*) decomposes a circuit that does not

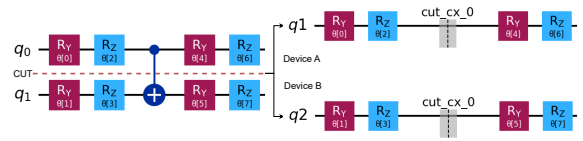


Figure 1: Independent subcircuits generated by cutting a circuit. The dashed line indicates the cut location; the resulting fragments (left and right subcircuits) can be executed independently on smaller devices. Each cut exponentially increases the number of subexperiments and reconstruction terms.

fit a target backend into a collection of smaller subcircuits that do, at the cost of classical reconstruction and increased sampling complexity [9, 10, 11]. The core trade-off is structural: cutting reduces spatial requirements (qubits) while increasing the number of executions and the weight of post-processing [9, 10].

Practical toolflows typically involve three stages. First, a compiler or optimiser chooses cut locations and a decomposition strategy [10, 12]. Second, a set of subcircuits (often many variants induced by the decomposition) are executed and measured [10, 13]. Third, a classical reconstruction procedure aggregates sub-results into an estimate of the target quantity (e.g., an expectation value) [10, 11, 12]. Recent work shows that allowing classical communication between subcomponents can reduce overhead constants in certain settings [11], and that alternative cutting schemes based on randomised measurements provide different accuracy-cost trade-offs [13].

Importantly for systems evaluation, cutting turns a single “large” circuit evaluation into a *task graph* with (often) substantial fan-out followed by a global aggregation. This introduces obvious bottleneck candidates: scheduling overhead, straggler sensitivity across large job sets, and a potentially heavy reduction (reconstruction) stage [10, 12]. These are precisely the failure modes we can only resolve by measured profiling rather than by asymptotic overhead counts alone.

The overhead scaling of circuit cutting is exponential in the number of cuts: each additional cut multiplies the number of required subexperiments and reconstruction terms. For  $c$  cuts across CNOT gates, the number of subexperiments grows as  $O(9^c)$  in the wire-cutting decomposition employed by *qiskit-addon-cutting* [18, 10], and the classical reconstruction cost scales correspondingly. This exponential growth has profound practical consequences that we quantify empirically in our evaluation (Section 5).

#### 2.1.4. Distributed Execution, Stragglers, and Staged Pipelines

Distributed systems research has repeatedly shown that scalability is frequently capped by coordination and stragglers rather than by idealised parallel work. MapReduce made this explicit, and speculative execution policies (e.g., LATE) were introduced specifically to mitigate heterogeneous task runtimes [6, 7]. In-memory dataflow systems and cluster computing abstractions (e.g., resilient distributed datasets) improved throughput for iterative workloads but still expose similar scheduling and reduction bottlenecks [31]. General-purpose task-graph engines such as Ray provide dynamic execution with task/actor abstractions that are well-suited to large ensembles of fine-grained jobs [16], while Python-native schedulers (e.g., Dask) emphasise blocked algorithms and dynamic task scheduling for scientific workloads [32].

Distributed machine learning (ML) provides a particularly relevant analogue. Parameter-server designs and consistency models were developed to manage synchronisation and straggler effects in synchronous and bounded-asynchrony regimes [33, 34]. Lock-free and asynchronous update schemes can improve throughput when assumptions (e.g., sparsity) hold, but they trade determinism for performance [35]. Data-parallel training commonly relies on collective communication (e.g., all-reduce), where communication structure and hierarchy-aware decomposition directly impact scaling [8, 36]. Even when compute parallelises cleanly, aggregation phases can dominate at scale [37, 8]. Work stealing provides a classic lens for understanding load balancing under irregular parallelism [38].

Circuit cutting produces a staged pipeline with the same fundamental shape: embarrassingly parallel sub-circuit execution followed by a global reconstruction. Therefore, the relevant question is not whether parallelism exists, but whether reconstruction and coordination costs dominate the critical path as we scale out [10, 7, 8]. Our evaluation is designed to quantify this boundary empirically.

### 2.2. Related Work

We organise related work into (i) circuit cutting methods and their overhead models, (ii) hybrid software stacks and execution interfaces, and (iii) distributed systems techniques for scaling estimator-heavy workloads.

#### 2.2.1. Circuit Cutting Methods, Overheads, and Optimisation Targets

Peng et al. [9] introduced a cluster simulation view that makes explicit how limited quantum memory can

be traded for exponential overhead in structural parameters, motivating decomposition as a route to execute circuits beyond device width. CutQC [10] provided an end-to-end toolflow that automates cut selection and reconstruction, and it documented that classical post-processing and the number of required subcircuits can grow rapidly with number and type of cuts. Subsequent work studied overhead reductions via classical communication [11] and via randomised measurement strategies that change the sampling profile [13]. More recently, the optimisation objective itself has been formalised: Harrow et al. [12] study optimality notions for cuts and provide bounds and constructions that clarify when overhead is unavoidable.

A complementary line of work investigates multi-processor or modular execution, including demonstrations combining multiple quantum processors with real-time classical coordination, alongside circuit cutting and dynamic control flow [39]. Industrial toolchains also explore serverless and managed execution environments for cutting workloads, reflecting an implicit acknowledgement that orchestration and classical processing are first-order concerns [40, 41, 42].

However, much of the circuit-cutting literature reports overhead primarily in terms of *counts* (numbers of subcircuits, asymptotic reconstruction complexity, sampling blow-up) rather than in terms of *measured* end-to-end time attribution on a distributed runtime. This limits our ability to understand when reconstruction becomes the bottleneck, how stragglers shape tail latency, and whether scheduling policies (e.g., staggering) materially affect throughput in practice.

#### 2.2.2. Hybrid Stacks and Estimator-Oriented Interfaces

The software ecosystem for hybrid execution has matured significantly. Qiskit [27] provides a widely used compilation and execution stack, and its design decisions and core components have been documented in a citable form suitable for systems and methodology discussion. Qiskit’s primitives [28] make expectation-value estimation and sampling explicit in the programming model. PennyLane [29] and TensorFlow Quantum [30] integrate quantum circuit evaluation into differentiable programming and ML workflows, providing interfaces that naturally generate estimator-heavy execution patterns. These stacks enable rapid prototyping, but they generally do not provide a systems-level analysis of distributed bottlenecks for cutting-plus-training pipelines; instead, performance is often reported at level of circuit runtime or simulator throughput [30, 29].

On the algorithmic side, error mitigation and hybrid methods emphasise that practical near-term execution

requires additional classical processing and repeated circuit evaluations [5, 3]. VQA surveys highlight that measurement cost and optimiser query complexity are central constraints [2, 20]. Yet, the interaction between these algorithmic requirements and distributed execution policies is typically left implicit. Our work treats this interaction as the primary object of measurement.

### 2.2.3. Distributed ML and Straggler-Aware Scheduling

Distributed ML provides established methods and cautionary lessons. Parameter-server architectures and bounded-staleness models reduce idle time under heterogeneity while maintaining correctness guarantees under controlled delay [33, 34]. Speculative execution strategies mitigate tail latency in large job sets [7], and general task-graph engines scale fine-grained workloads by separating control and data planes [16]. Communication libraries and all-reduce decompositions show that collective aggregation can dominate and that topology-aware design is critical [8, 36]. Large-batch scaling studies reinforce that synchronisation and communication, not just computation, control speed-up at scale [37].

Robustness and stability further motivate careful evaluation. Classical adversarial robustness work demonstrates that training dynamics and optimisation procedures materially affect robustness properties [43, 44, 14, 15]. In estimator-heavy quantum-classical training, analogous concerns arise from sampling noise, estimator variance, and distribution shifts induced by decomposition choices, which can alter optimisation trajectories even when the target function is theoretically preserved [2, 4, 3]. Existing work rarely connects these robustness/stability questions to the systems bottlenecks introduced by cutting and reconstruction.

### 2.3. Summary and Gap

Prior work establishes that circuit cutting can extend executable circuit sizes [9, 10], and it clarifies key overhead trade-offs and potential reductions [11, 13, 12]. In parallel, hybrid software stacks expose estimator-oriented execution models [27, 28, 29, 30], while distributed systems research provides mature techniques for reasoning about stragglers and aggregation bottlenecks [6, 7, 33, 8]. What remains underexplored is a measurement-driven, system-level account of how cutting transforms end-to-end training into a staged distributed pipeline, when reconstruction dominates, and which execution policies materially improve throughput without degrading accuracy or robustness. Our paper addresses this gap by instrumenting and attributing

costs across cutting, subcircuit execution, reconstruction, and training dynamics under controlled distributed execution.

## 3. System Model and Problem Formulation

In this section, we formalise the estimator-driven, cut-aware training pipeline as a staged distributed computation and define measurable performance and outcome quantities aligned with our research questions (RQ1–RQ5).

### 3.1. End-to-End Pipeline Model

Figure 2 shows the pipeline we evaluate. A classical dataset is preprocessed and supplied to a training loop. Each iteration evaluates a quantum neural network (QNN) forward pass and associated loss, and updates parameters via a classical optimiser. The forward pass is implemented via expectation estimation queries of the form  $(C(\theta, x), O)$ , where  $C$  is a parameterised circuit instantiated at parameters  $\theta$  and input  $x$ , and  $O$  is the observable (or set of observables) required to compute model outputs and loss [2, 4].

When circuit cutting is enabled, the estimator query is expanded into a set of subexperiments that can be executed independently, followed by a classical reconstruction step that returns the estimate to the training loop [10, 9, 12]. This transformation is central to our study because it introduces (i) additional overheads beyond baseline execution (RQ1), (ii) a reconstruction barrier that can dominate the critical path under scale-out (RQ2), and (iii) scheduling degrees of freedom, including staggering, that affect straggler sensitivity and throughput (RQ3). The same transformation may also affect learning dynamics through estimator variance and evaluation order, which we examine through accuracy and robustness outcomes (RQ4–RQ5).

### 3.2. Integration with QML Training Loop

To make the integration between the cut-aware pipeline and the QML training loop precise, we describe the data and control flow through the key software components.

The parameterised quantum circuit  $C(\theta, x)$  and observable  $O$  are encapsulated in an *EstimatorQNN* instance [17], which exposes a differentiable forward pass and gradient computation interface. The *TorchConnector* wraps this *EstimatorQNN* as a PyTorch `nn.Module`, enabling standard PyTorch optimisers (e.g., Adam) and loss functions (e.g., cross-entropy) to be used without modification.

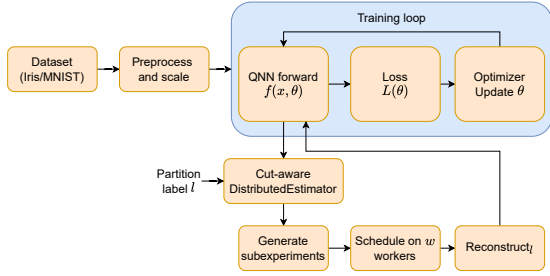


Figure 2: Training pipeline with a cut-aware distributed estimator. Circuit cutting expands each estimator query in the QNN forward/gradient evaluation into parallel subexperiments followed by classical reconstruction. The pipeline stages are colour-coded: data preprocessing (left), QNN training loop (centre), and the cut-aware estimator expansion (right) comprising partitioning, parallel execution, and reconstruction.

During the forward pass, *TorchConnector* calls *EstimatorQNN.forward()*, which internally issues one or more estimator queries  $(C(\theta, x_i), O)$  for each input sample  $x_i$  in the current batch. In the baseline (no-cut) configuration, each query is evaluated directly by the Aer simulator backend. When cutting is enabled, our *DistributedEstimator* intercepts these queries and processes each one through the staged pipeline described below.

For gradient computation, the *EstimatorQNN* uses the parameter-shift rule [4]: for each trainable parameter  $\theta_j$ , two additional estimator queries are issued with  $\theta_j \pm \pi/2$ . Each of these shifted queries is independently processed through the same cut-aware pipeline, producing reconstructed expectation values that are combined to compute the gradient  $\partial\langle O \rangle / \partial\theta_j$ . The gradients are returned to *TorchConnector*, which passes them to PyTorch’s autograd engine for backpropagation through any classical layers and the optimiser update step.

This design has two important properties. First, the cut-aware estimator is transparent to the optimiser: gradients computed via the parameter-shift rule with cutting are mathematically equivalent to those without cutting (up to finite-sample variance differences), ensuring that the optimiser receives unbiased gradient estimates. Second, the overhead of cutting is multiplicative at the estimator-query level: if the forward pass for one sample requires  $q$  estimator queries and the parameter-shift gradient requires  $2p$  additional queries (for  $p$  parameters), then the total number of cut-aware estimator invocations per training iteration is  $(q + 2p) \times |\text{batch}|$ , each of which expands into  $K$  subexperiments. This multiplicative expansion is the root cause of the training time overheads documented in RQ1.

### 3.3. Cut-Aware Estimator Query Model

For a single query instance  $(C(\theta, x), O)$ , circuit cutting produces a partition labelled by  $\ell$  and yields subcircuits and subobservables. The resulting execution requires a finite set of concrete subexperiments  $\mathcal{E} = \{e_k\}_{k=1}^K$  and reconstruction coefficients  $\alpha$  determined by the cutting scheme and partition [10, 12]. Each  $e_k$  is executed with a fixed shot count  $S$ , producing a classical summary  $r_k$  (e.g., outcome counts). Reconstruction aggregates  $\mathcal{R} = \{r_k\}$  into an estimate  $\hat{y}$  of the target expectation value.

This induces a staged cost decomposition for each query instance:

$$T_{\text{total}} = T_{\text{part}} + T_{\text{gen}} + T_{\text{exec}} + T_{\text{rec}}, \quad (1)$$

where:

- $T_{\text{part}}$  is circuit/observable partitioning time (including cut planning and partition materialisation);
- $T_{\text{gen}}$  is subexperiment generation time (including basis variants and reconstruction coefficients);
- $T_{\text{exec}}$  is parallel execution time of  $\mathcal{E}$  on a worker pool;
- $T_{\text{rec}}$  is classical reconstruction time.

Eq. (1) provides the measurement backbone for RQ1 and RQ2: we report each component as a measured quantity and study how their shares evolve with the degree of parallelism.

### 3.4. Execution, Stragglers, and Scheduling

We model subexperiment execution as a set of independent tasks scheduled on  $w$  workers, followed by a reconstruction barrier. Figure 3 captures this per-query expansion and the straggler sensitivity introduced by the barrier. Let  $t_k$  denote the service time for subexperiment  $e_k$  (including dispatch and backend runtime). Under a work-conserving policy, the realised parallel time is governed by load balance and tail effects and can be expressed as:

$$T_{\text{exec}} \approx \max_{i \in \{1, \dots, w\}} \sum_{k \in \mathcal{A}(i)} t_k, \quad (2)$$

where  $\mathcal{A}(i)$  is the assignment of subexperiments to worker  $i$ . This form makes explicit why speed-up can saturate even when the task set is abundant:  $T_{\text{exec}}$  is bounded by the slowest worker, and  $T_{\text{rec}}$  is a serial reduction that must wait for all results, mirroring classical bottlenecks in staged distributed computations [6, 7].

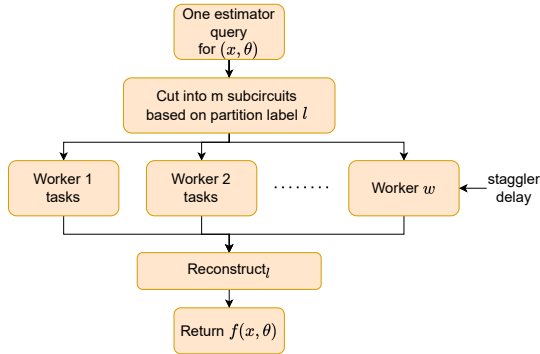


Figure 3: Per-query expansion under circuit cutting. Subexperiments (shown as shaded blocks) execute across  $w$  workers; reconstruction (dark block) forms a barrier. Straggler delays (hatched blocks) on individual workers extend the critical path, delaying the reconstruction barrier.

To study straggler sensitivity repeatedly, we allow an optional synthetic delay process at the task level. Each subexperiment independently incurs an injected delay  $\Delta$  with probability  $p$ , yielding  $t'_k = t_k + \mathbf{1}\{u_k < p\}\Delta$  for  $u_k \sim \text{Uniform}(0, 1)$ . We use this mechanism strictly as an experimental control to stress the tail of Eq. (2) and to evaluate whether scheduling choices (including staggering) reduce end-to-end time-to-solution under heterogeneity [7].

### 3.5. Problem Definition

We consider a fixed training protocol (dataset split, optimiser, stopping criterion) and a fixed per-subexperiment shot budget  $S$ . For a given configuration (cut plan  $\ell$ , worker pool size  $w$ , scheduling policy  $\pi$ , and optional straggler parameters), our primary systems objective is to minimise *time-to-solution* while preserving learning outcomes:

$$\min_{\pi \in \Pi} \mathbb{E}[T_{\text{total}}] \quad \text{s.t.} \quad \text{accuracy and robustness constraints.} \quad (3)$$

We operationalise this objective through:

- *Measured*:  $T_{\text{part}}, T_{\text{gen}}, T_{\text{exec}}, T_{\text{rec}}, T_{\text{total}}$  per query instance (and their aggregation over training);
- *Derived*: stage shares (e.g.,  $T_{\text{rec}}/T_{\text{total}}$ ), scaling curves as a function of  $w$ , and bottleneck attribution via changes in dominant stage across configurations;
- *Observed*: training outcomes (accuracy) and robustness metrics computed under a consistent evaluation regime.

This mapping directly supports RQ1–RQ5: overhead and scaling are answered by timing breakdowns and their evolution with  $w$ ; the existence of a reconstruction bottleneck is established by measured dominance of  $T_{\text{rec}}$  and the saturation of speed-up; the impact of staggering is established by changes in  $T_{\text{exec}}$  tail behaviour and  $T_{\text{total}}$ ; and outcome preservation is established by measured accuracy and robustness under unchanged training and evaluation procedures.

## 4. Methodology

In this section, we describe how we implement the cut-aware distributed estimator, how we instrument stage-level timings and outcomes, and how we configure scheduling policies and straggler controls to answer RQ1–RQ5.

### 4.1. Cut-Aware Distributed Estimator

Our estimator backend implements a cut-aware execution path that transforms each query instance  $(C(\theta, x), O)$  into a set of subexperiments and a reconstruction plan. Concretely, for each query instance we: (i) partition the problem according to a partition label  $\ell$ , (ii) generate the concrete subexperiments  $\mathcal{E}$  and reconstruction coefficients  $\alpha$ , (iii) execute  $\mathcal{E}$  across a worker pool of size  $w$ , (iv) reconstruct the target estimate  $\hat{y}$ , (v) return  $\hat{y}$  to the training loop.

The key methodological choice is to treat this as a *staged* pipeline and to instrument each stage individually. This allows us to attribute overheads introduced by cutting (RQ1) and to identify scaling limits caused by reconstruction and coordination (RQ2) without conflating them with training-loop compute.

Algorithm 1 summarises the per-query logic. The algorithm is intentionally phrased to align with logged quantities and the timing decomposition in Eq. (1).

### 4.2. Scheduling Policies and Staggering

We evaluate execution policies that differ in how they submit and allocate the task set  $\mathcal{E}$  to a bounded worker pool of size  $w$ . We consider three dispatch strategies:

1. **Eager dispatch**: All subexperiments in  $\mathcal{E}$  are submitted to the worker pool immediately. The runtime uses a work-conserving, first-come-first-served allocation. This is the simplest policy and serves as our baseline scheduling strategy.
2. **Batched dispatch**: Subexperiments are partitioned into batches of size  $B$  and submitted sequentially with an inter-batch delay  $\delta$ . This policy controls the degree of concurrent submissions and can

---

**Algorithm 1** Instrumented cut-aware estimator for one query instance

---

**Require:** Circuit  $C(\theta, x)$ , observable  $O$ , partition label  $\ell$ , shots  $S$ , workers  $w$ , scheduling policy  $\pi$

- 1: Initialise timers and metadata record
- 2: **Partition:**  
 $(\{C_i\}, \{O_i\}, \mathcal{B}) \leftarrow \text{PartitionProblem}(C, O, \ell)$
- 3: **Generate:**  
 $(\mathcal{E}, \alpha) \leftarrow \text{GenerateSubexperiments}(\{C_i\}, \{O_i\}, S)$
- 4: **Execute:**  $\mathcal{R} \leftarrow \text{ExecuteTasks}(\mathcal{E}, w, \pi)$
- 5: **Reconstruct:**  $\hat{y} \leftarrow \text{Reconstruct}(\mathcal{R}, \alpha, \{O_i\}, O)$
- 6: Log  $(T_{\text{part}}, T_{\text{gen}}, T_{\text{exec}}, T_{\text{rec}}, T_{\text{total}})$  and metadata to JSONL
- 7: **return**  $\hat{y}$

---

reduce transient contention when the worker pool or backend has limited capacity.

3. **Staggered dispatch:** Subexperiments are grouped by partition label or structural similarity and submitted in a deliberately spaced sequence. The intent is to reshape the arrival pattern to avoid correlated queueing delays that can arise when structurally similar subexperiments compete for the same resources.

All three policies terminate in the same reconstruction barrier: the training loop does not proceed until all subexperiment results are available. The key difference is in how they shape the distribution of  $T_{\text{exec}}$ , particularly its tail. A policy that reduces the variance of individual task completion times can lower the expected value of  $\max_i \sum_{k \in \mathcal{A}(i)} t_k$  and thereby reduce  $T_{\text{exec}}$ , even if it does not change the total work.

Algorithm 2 gives a generic dispatch routine that captures eager, batched, and staggered submission as special cases via the policy  $\pi$ .

We note that our current evaluation focuses primarily on the eager dispatch policy with straggler injection to stress the tail of  $T_{\text{exec}}$  (RQ3). A comprehensive comparison of batched and staggered policies under varying  $B$ ,  $\delta$ , and task ordering rules is an important direction for future work, as discussed in Section 6. The framework and instrumentation support this extension: all dispatch parameters are logged alongside stage-level timings, enabling post-hoc attribution of throughput and tail-latency changes to specific scheduling choices.

### 4.3. Straggler Control

When enabled, synthetic straggler injection is applied at task execution time. Each subexperiment independently incurs an additional delay  $\Delta$  with prob-

---

**Algorithm 2** Task dispatch with configurable scheduling policy

---

**Require:** Task set  $\mathcal{E}$ , workers  $w$ , policy  $\pi$  (batch size  $B$ , inter-batch delay  $\delta$ , ordering rule)

- 1: Order tasks  $\mathcal{E}$  according to  $\pi$  (e.g., FIFO, grouped by label)
- 2: Partition ordered tasks into batches  $\{\mathcal{E}^{(b)}\}$  of size  $B$  (or one batch if eager)
- 3: **for** each batch  $\mathcal{E}^{(b)}$  **do**
- 4:   Submit all  $e_k \in \mathcal{E}^{(b)}$  to the worker pool; collect futures
- 5:   **if**  $\delta > 0$  **then**
- 6:     Sleep for  $\delta$
- 7:   **end if**
- 8: **end for**
- 9: Wait for all tasks; return results  $\mathcal{R}$

---

ability  $p$ , yielding  $t'_k = t_k + \mathbf{1}\{u_k < p\}\Delta$ . This allows us to stress the barrier sensitivity in Fig. 3 and evaluate whether the critical-path structure (execution-dominated vs. reconstruction-dominated) modulates straggler impact (RQ3). We log injected delays alongside per-stage timings to ensure that straggler effects are explicitly traceable in subsequent analysis.

### 4.4. Instrumentation and Outcome Tracking

For each estimator query, we emit a JSONL record containing: (i) query structure (e.g., number of subexperiments  $K$ , shots  $S$ ), (ii) configuration (partition label  $\ell$ , worker pool size  $w$ , scheduling policy identifier, straggler parameters when enabled), and (iii) measured stage timings consistent with Eq. (1). At the training level, we log loss traces, optimiser steps, and evaluation metrics.

This instrumentation supports:

- *RQ1*: compare baseline vs. cut variants via differences in  $(T_{\text{part}} + T_{\text{gen}} + T_{\text{rec}})$  and changes in  $T_{\text{exec}}$  under matched shot budgets;
- *RQ2*: attribute scaling saturation to dominant stage shares and reconstruction-barrier behaviour;
- *RQ3*: quantify the effect of scheduling policy and straggler injection on  $T_{\text{exec}}$  tail behaviour and end-to-end  $T_{\text{total}}$ ;
- *RQ4–RQ5*: evaluate whether accuracy and robustness metrics are preserved under identical training and evaluation procedures, and relate any changes to measured estimator-stage behaviour rather than untracked confounders.

## 5. Performance Evaluation

We evaluate the proposed cut-aware estimator pipeline using instrumented execution traces to quantify end-to-end overheads, scaling behaviour, sensitivity to injected stragglers, and learning outcomes (accuracy and robustness). All claims in this section are grounded in measured quantities recorded in the run-level records, estimator-call summaries, and robustness traces.

### 5.1. Experimental Setup

**Software stack.** All experiments are implemented in Python. Quantum circuits are constructed in Qiskit [45] and executed using the Aer primitive interface (SamplerV2/AerSampler, depending on the installed *qiskit-aer* version). Circuit cutting is implemented with *qiskit-addon-cutting* [18] via the standard decomposition workflow, which performs wire cutting through CNOT gate decomposition. The learning pipeline uses *qiskit-machine-learning* (EstimatorQNN and TorchConnector [17]) and PyTorch for optimisation; MNIST [46] data handling uses Torchvision, and Iris [47] preprocessing uses scikit-learn. The distributed execution model uses a bounded thread-based worker pool, with the worker count logged as *subexp\_workers* (MNIST) or *max\_subexp\_workers* (Iris).

**Model circuits.** Across both workloads, we instantiate a parameterised quantum circuit as the composition of a *ZFeatureMap* (encoding classical features into qubit rotations) followed by a *RealAmplitudes* ansatz with one repetition (*reps*=1), which provides a hardware-efficient parameterisation of the unitary search space. For Iris, the observable is the tensor-product Pauli-Z operator  $Z^{\otimes n}$ , implemented as a *SparsePauliOp* with  $n$  qubits, yielding a scalar expectation-value classifier output. For MNIST, a similar observable structure is used. The choice of a single-repetition ansatz keeps the parameter count manageable while providing sufficient expressivity for the binary classification tasks considered.

**Workloads and training budgets.** We consider two binary classification tasks: *iris\_binary\_pm1* (two classes from the Iris dataset, labels mapped to  $\pm 1$ ) and *mnist\_binary* (two-digit binary classification from MNIST). We enforce matched comparisons within each dataset by fixing the estimator shot budget (1024 shots per (sub)experiment) and by restricting comparisons to runs executed under the same training budget and straggler configuration.

For the clean (non-straggler) setting, we report results using the longest training budgets available for each dataset (Iris: *maxiter* = 60; MNIST: 10 epochs),

with *straggler\_delay\_s*= 0.0. For scaling analysis, shorter budgets are used (Iris: *maxiter* = 10; MNIST: 5 epochs), again with *straggler\_delay\_s*= 0.0, to match the worker-count sweeps used in our scaling experiments. For straggler sensitivity, we inject delays of *straggler\_delay\_s*= 0.1; these experiments use Iris with *maxiter* = 10 and MNIST with 3 epochs at 8 workers.

**Computational cost and qubit-count scope.** The computational cost of training hybrid quantum models with circuit cutting grows exponentially with the number of cuts. In the wire-cutting decomposition used by *qiskit-addon-cutting*, each cut across a CNOT gate decomposes the gate into nine subexperiment variants, yielding a multiplicative overhead of  $O(9^c)$  for  $c$  cuts [18, 10]. This means that a circuit with one cut requires  $9\times$  more subexperiments than the uncut baseline, two cuts require  $81\times$ , and three cuts require  $729\times$ . In addition to the subexperiment count, the classical reconstruction cost and the intermediate state that must be stored and processed grow correspondingly.

This exponential scaling renders experiments beyond 4 qubits computationally prohibitive within practical time budgets. A single higher-qubit configuration with cutting would require orders-of-magnitude more computation than the 4-qubit configurations evaluated here, making systematic sweeps over seeds, cut counts, and worker configurations impractical. We therefore restrict our evaluation to circuits with up to 4 qubits, which is representative of the scale at which circuit cutting is currently applied in practice [10, 12]. Our findings about reconstruction dominance and scaling saturation are structural properties of the pipeline that become more pronounced at larger scales, since both the subexperiment count and the reconstruction workload grow exponentially.

**Logging and derived metrics.** We instrument each run to record end-to-end training time, test accuracy, stage-level timings (subexperiment execution and classical reconstruction durations per estimator call), and robustness traces under injected Gaussian noise and FGSM perturbations at multiple perturbation magnitudes. From these measurements, we report total training time as well as the fraction of time spent in reconstruction versus subexperiment execution. Scaling and straggler sensitivity ratios are computed only between runs matching dataset, seed, model configuration, and cut label, ensuring that observed differences are attributable to the varied parameter (worker count or straggler rate) rather than to confounding factors.

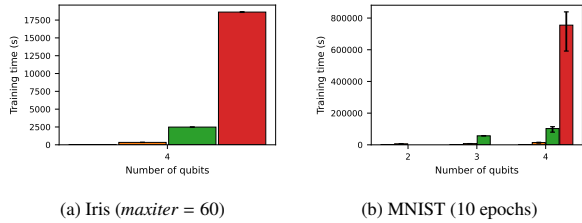


Figure 4: RQ1: End-to-end training time under clean execution. Legend: blue = no cut, orange = 1 cut, green = 2 cuts, red = 3 cuts. Training time increases substantially with cut count due to subexperiment expansion and reconstruction overhead.

## 5.2. Results and Analysis

### 5.2.1. RQ1: Cutting Overhead

Figure 4 reports end-to-end training time under the clean setting with the maximum training budgets (Iris:  $maxiter = 60$ ; MNIST: 10 epochs). Across both datasets, training time increases sharply with cut count, consistent with the  $O(9^c)$  subexperiment expansion compounded across all estimator queries in the training loop. Because the parameter-shift gradient rule doubles the number of estimator queries per parameter, the total computational cost per training iteration scales as  $(q+2p) \times \text{batch} \times 9^c$  subexperiments, where  $q$  is the number of forward-pass queries,  $p$  is the parameter count, and  $c$  is the number of cuts. The observed training time growth is therefore not a small constant surcharge but a multiplicative workload expansion that compounds across all estimator invocations in each training iteration.

For the MNIST workload, the training time increase from no cut to three cuts is approximately an order of magnitude, reflecting the combined effect of  $729 \times$  more subexperiments per estimator query and the corresponding growth in reconstruction work. On Iris, the relative overhead is also substantial but lower in absolute terms due to the smaller dataset and training budget.

### 5.2.2. RQ2: Scalability Bottlenecks

Figure 5 reports speed-up from increasing parallelism, defined as the ratio of training time at 1 worker to training time at 16 workers, computed only for matched seed–configuration pairs. For MNIST (5 epochs, clean), speed-ups are close to or below 1, indicating that additional workers do not yield proportional time reductions. Iris shows the same qualitative behaviour under  $maxiter = 10$ .

The worker pool size  $w$  controls only the concurrent subexperiment execution within the *ExecuteTasks* phase of Algorithm 1. It does not affect the serial partitioning,

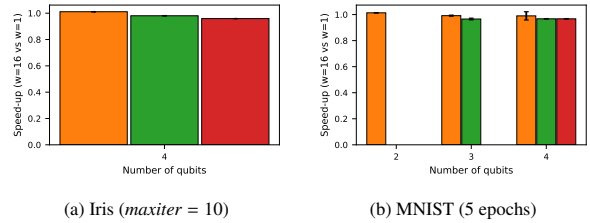


Figure 5: RQ2: Scaling behaviour under clean execution. Legend: blue = no cut, orange = 1 cut, green = 2 cuts, red = 3 cuts. Bars report speed-up at 16 workers relative to 1 worker for matched pairs. Speed-up near or below 1 indicates reconstruction overhead dominates.

Table 1: RQ2: Reconstruction share ( $T_{rec}/T_{total}$ ) from estimator-call summaries under clean execution ( $straggler\_delay\_s = 0.0$ ). The monotonic increase with cut count confirms that reconstruction progressively dominates per-query time.

#cuts	$n$	median $T_{rec}/T_{total}$	p95 $T_{rec}/T_{total}$
1	41	0.430	0.474
2	28	0.489	0.533
3	5	0.530	0.580

generation, or reconstruction phases. When  $T_{rec}$  dominates (as in higher-cut configurations), increasing  $w$  has diminishing returns regardless of the available parallelism in execution. This is a direct instance of Amdahl’s law: the serial reconstruction fraction places an upper bound on achievable speed-up that no amount of execution parallelism can overcome.

Table 1 quantifies the reconstruction share from estimator-call summaries: the ratio  $T_{rec}/T_{total}$  computed from per-call timing records. Reconstruction accounts for a substantial and monotonically increasing fraction of per-query time as cuts increase. At one cut, the median reconstruction share is 43%; at two cuts it rises to 49%; and at three cuts it reaches 53% (with a 95th percentile of 58%). This means that even with hypothetically perfect parallelisation of the entire execution phase (reducing  $T_{exec}$  to zero), the total query time at three cuts could be reduced by at most 47%. In practice, since  $T_{exec}$  cannot be fully eliminated, the achievable speed-up is even more limited. This reconstruction barrier is the primary mechanism explaining the scaling saturation observed in Fig. 5.

### 5.2.3. RQ3: Straggler Sensitivity

Figure 6 reports sensitivity to injected stragglers ( $straggler\_delay\_s = 0.1$ ), showing the slowdown ratio at straggler probability  $p = 0.2$  relative to  $p = 0.0$ . A ratio greater than 1 indicates that stragglers increase total training time; the magnitude indicates how much.

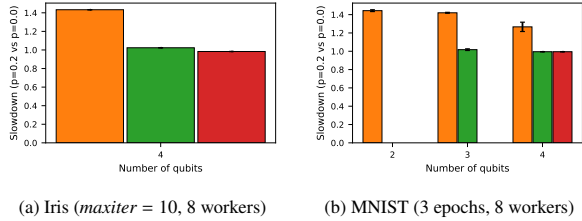


Figure 6: RQ3: Straggler sensitivity at  $straggler\_delay\_s = 0.1$ . Legend: blue = no cut, orange = 1 cut, green = 2 cuts, red = 3 cuts. Bars report slowdown at  $p = 0.2$  relative to  $p = 0.0$ . Reconstruction-dominated configurations show lower sensitivity to execution-side stragglers.

The resulting slowdowns vary across configurations in a manner consistent with the staged pipeline model. Configurations where reconstruction dominates the critical path exhibit *lower* relative sensitivity to execution-side stragglers: since  $T_{rec}$  is unaffected by execution delays, the additional time from stragglers constitutes a smaller fraction of the already-large  $T_{total}$ . Conversely, configurations with a larger execution share ( $T_{exec}/T_{total}$ ) amplify tail latency more strongly, because the reconstruction barrier must wait for all subexperiments to complete, and the slowest straggler determines  $T_{exec}$ .

This finding has a practical implication for system design: straggler mitigation strategies such as speculative execution [7] or work stealing [38] are most effective when applied to configurations where  $T_{exec}$  constitutes a significant fraction of  $T_{total}$ . In reconstruction-dominated regimes, reducing execution-side variance yields diminishing returns, and effort is better directed towards reducing or overlapping the reconstruction phase itself.

#### 5.2.4. RQ4: Accuracy

Figure 7 reports test accuracy under the clean setting with the maximum training budgets (Iris:  $maxiter = 60$ ; MNIST: 10 epochs).

On Iris, all evaluated configurations—including no-cut, one-cut, two-cut, and three-cut settings—achieve identical test accuracy, confirming that circuit cutting does not degrade predictive performance for this task. This result is expected given that reconstruction is mathematically exact (up to finite-sample variance), and the Iris classification task is sufficiently low-dimensional that the optimiser converges to the same solution regardless of the estimator variance introduced by cutting.

On MNIST, accuracy varies with qubit descriptor and random seed, reflecting the higher-dimensional optimisation landscape and greater sensitivity to initialisation

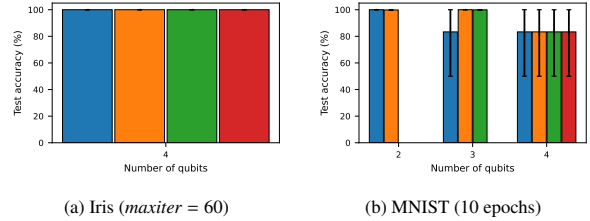


Figure 7: RQ4: Absolute test accuracy under clean execution. Legend: blue = no cut, orange = 1 cut, green = 2 cuts, red = 3 cuts. On Iris, accuracy is invariant across cut settings. On MNIST, accuracy is not systematically degraded by cutting.

and estimator noise. However, no systematic degradation is observed as cut count increases: several cut configurations achieve accuracy comparable to or higher than the no-cut baseline under the same training budget. This behaviour is consistent with the observation that cutting changes the effective noise profile of the estimator—the aggregation of multiple subexperiment results can introduce different variance characteristics compared to a single circuit evaluation—which can alter optimisation trajectories even when the expected value of the reconstructed estimate is unbiased. These trajectory differences are configuration-dependent and can occasionally lead to improved final accuracy by effectively regularising the optimisation through increased estimator noise.

#### 5.2.5. RQ5: Robustness

We evaluate robustness using perturbation traces under two complementary attack models: additive Gaussian noise (random perturbations to input features) and Fast Gradient Sign Method (FGSM) attacks [44] (adversarial perturbations along the gradient direction). Figure 8 reports a robustness summary per run, computed as the mean accuracy over non-zero perturbation magnitudes averaged across both attack types.

For Iris, the robustness summary matches the clean accuracy across all configurations, indicating no measurable robustness degradation due to cutting. This is consistent with the accuracy invariance observed in RQ4 and suggests that the Iris models’ decision boundaries are sufficiently robust that neither the cutting-induced estimator noise nor the adversarial perturbations at the tested magnitudes are sufficient to alter predictions.

For MNIST, robustness varies across configurations, but several cut configurations achieve robustness comparable to the baseline, and some exhibit improved robustness within the measured runs. The observation that cutting can sometimes improve robustness is con-

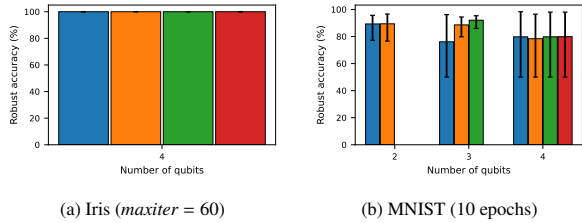


Figure 8: RQ5: Robustness summary under clean execution. Legend: blue = no cut, orange = 1 cut, green = 2 cuts, red = 3 cuts. Bars report mean accuracy over non-zero perturbation magnitudes (Gaussian and FGSM). Robustness is not systematically degraded by cutting.

sistent with the noise-regularisation interpretation: the increased estimator variance during training may produce models with smoother decision boundaries that are less sensitive to small input perturbations [14]. However, given the limited number of seeds per configuration, we report these effects as measured outcomes and note that a more extensive evaluation would be needed to establish the robustness improvement as a reliable effect.

## 6. Discussion and Future Work

Our evaluation demonstrates that circuit cutting should be treated as a staged distributed workload rather than a purely algorithmic transformation. The central observation across RQ1–RQ3 is that, while cutting increases parallelisable work, it simultaneously introduces substantial non-parallel components—particularly reconstruction—that dominate end-to-end performance. This section consolidates these findings, discusses the practical implications, and outlines future directions.

### 6.1. Discussion

**Reconstruction is the primary scaling limiter.** RQ2 quantifies reconstruction as a substantial and growing share of per-query time (53% median at three cuts), inducing two scaling constraints. First, the serial reconstruction stage bounds achievable speed-up even under ideal execution parallelism—a direct instance of Amdahl’s law applied to the cut-aware pipeline. If we denote the serial (reconstruction) fraction as  $f$ , the maximum achievable speed-up with  $w$  workers is bounded by  $1/(f + (1-f)/w)$ , which converges to  $1/f$  as  $w \rightarrow \infty$ . At  $f = 0.53$  (three cuts, median), this yields a maximum theoretical speed-up of approximately 1.89 $\times$ , regardless of how many workers are available. Second, reconstruction acts as a global barrier: the training loop does not progress until all subexperiment results are available,

making the pipeline sensitive to upstream tail latency. These effects explain the speed-up saturation observed in Fig. 5 and indicate that reducing the reconstruction fraction is a prerequisite for meaningful parallel scaling.

**The  $O(9^c)$  overhead compounds across training.** A key insight from RQ1 is that the exponential subexperiment overhead is not incurred once per training run but rather once per estimator query. Because the parameter-shift gradient rule generates  $2p$  shifted queries per iteration (for  $p$  trainable parameters) in addition to the forward-pass queries, and each query independently undergoes the  $9^c$ -fold expansion, the total number of subexperiments per training epoch scales as  $O(9^c \cdot p \cdot |\text{dataset}|)$ . This compounding effect is the primary reason that training time increases by an order of magnitude at three cuts: even though each individual subexperiment is a small quantum job, the combinatorial explosion in the number of such jobs dominates total wall-clock time.

**Straggler sensitivity is modulated by critical-path structure.** RQ3 shows that configurations dominated by reconstruction exhibit lower sensitivity to execution-side delays, whereas configurations with a larger execution share amplify tail latency more strongly. This has a direct practical implication: the optimal mitigation strategy depends on where the bottleneck currently lies. In execution-dominated regimes, classical straggler mitigation (speculative execution, work stealing) is effective. In reconstruction-dominated regimes, the priority should shift to reconstruction optimisation—parallelising, approximating, or overlapping the reconstruction phase—rather than investing in more sophisticated execution scheduling.

**Learning outcomes are preserved under cutting.** RQ4 confirms that accuracy is fully preserved on Iris and not systematically degraded on MNIST across all evaluated cut configurations. RQ5 demonstrates that robustness under both Gaussian noise and FGSM adversarial perturbations is maintained, with some cut settings exhibiting comparable or improved robustness relative to the uncut baseline. These findings are practically significant because they validate that circuit cutting can be employed as a systems-level strategy to execute oversized circuits without silently degrading the quality of the trained model. The preservation of robustness is particularly notable, as it indicates that the noise introduced by cutting-based estimator decomposition does not create exploitable vulnerabilities in the learned decision boundaries.

**Implications for system design.** Taken together, our findings suggest several design principles for cut-aware quantum training systems: (i) the reconstruction

phase should be treated as a first-class optimisation target, not a fixed post-processing cost; (ii) scheduling policies should be aware of the reconstruction fraction and adapt their strategy accordingly; (iii) resource allocation between execution workers and reconstruction compute should be balanced rather than maximising execution parallelism alone; and (iv) the exponential overhead profile should inform decisions about when cutting is preferable to alternative approaches (e.g., model compression, shallower circuits, or waiting for larger devices).

### 6.2. Scope and Generalisability

We identify the following scope boundaries that contextualise our results.

**Experimental scale.** The  $O(9^c)$  growth of subexperiment counts restricts practical experimentation to small qubit counts with current CNOT-based wire-cutting methods. Our evaluation uses circuits with up to 4 qubits and two binary classification tasks, which is representative of the scale at which circuit cutting is currently applied [10, 12]. The structural findings—reconstruction dominance, scaling saturation, and straggler sensitivity patterns—are architectural properties of the pipeline that become more pronounced at larger scales, since the reconstruction share increases monotonically with cut count (Table 1).

**Runtime and evaluation scope.** Our implementation uses a thread-based worker pool rather than a fully distributed runtime, which isolates cut-aware pipeline effects from network and serialisation confounders. The qualitative findings are structural properties of the pipeline rather than threading artefacts. The number of independent runs per configuration, particularly for the 3-cut setting ( $n = 5$ ), limits the statistical power of individual comparisons; we report medians and 95th percentiles accordingly. The observed trends—increasing reconstruction share, preserved accuracy, and maintained robustness—are directionally consistent across all configurations and both datasets.

### 6.3. Future Work

**Minimising reconstruction overhead.** The most pressing direction is reducing the reconstruction bottleneck that currently limits both experimental scalability and practical deployment. Promising approaches include: (i) approximate reconstruction via tensor-network contractions or low-rank methods to reduce cost from exponential to polynomial in the number of cuts; (ii) distributed tree-reduction to parallelise the reconstruction phase itself, breaking the serial barrier;

(iii) incremental reconstruction that updates partial estimates as subexperiment results arrive, enabling overlap between late execution and early aggregation; and (iv) integration of reduced-overhead cutting schemes such as randomised cutting [13] and communication-enhanced cutting [11], which can reduce the base of the exponential from 9 to smaller constants.

**Scheduling policy design.** Our evaluation focused on eager dispatch with straggler injection. A systematic comparison of batched and staggered dispatch strategies, variance-aware schedulers that prioritise high-importance subexperiments, and adaptive shot allocation schemes would enable a more complete understanding of how scheduling policies interact with the reconstruction barrier. The instrumentation framework presented in this work directly supports such extensions.

**Extended evaluation scope.** Validating the key findings on a distributed runtime (e.g., Ray [16]), with hardware-backed QPU execution, additional datasets and ansatz depths, multi-class classification problems, and detailed convergence analysis (per-iteration loss curves) would strengthen the generalisability of our conclusions and clarify the boundary conditions under which cutting remains a viable strategy.

## 7. Conclusions

We proposed *DistributedEstimator*, a cut-aware estimator execution pipeline for training quantum neural networks via circuit cutting, and evaluated it as a staged distributed workload with explicit measurement of overheads, bottlenecks, and learning outcomes.

Our results demonstrate that circuit cutting introduces substantial end-to-end overheads that grow with cut count (RQ1). Classical reconstruction is a primary contributor to wall-clock time, reaching a median of 53% and a 95th percentile of 58% of per-query estimator time at three cuts, thereby limiting achievable speed-up under increased parallelism (RQ2). Straggler-induced tail effects measurably impact time-to-solution, with sensitivity governed by the balance between execution and reconstruction on the critical path (RQ3). Despite these systems costs, test accuracy is fully preserved on Iris and maintained without systematic degradation on MNIST across all evaluated cut configurations (RQ4). Robustness under Gaussian noise and FGSM perturbations is similarly preserved, with several cut configurations exhibiting comparable or improved robustness relative to the uncut baseline (RQ5).

The exponential growth of subexperiment counts with each additional cut ( $O(9^c)$ ) for CNOT-based wire

cutting) represents a fundamental computational barrier that constrains practical experimentation to small qubit counts with current methods. This motivates a focused effort on overhead reduction—through approximate reconstruction, distributed reduction, and reduced-overhead cutting schemes—as a prerequisite for scaling circuit cutting to practically relevant QML workloads. Overall, our study establishes that scalable circuit cutting for learning workloads requires treating reconstruction and aggregation as first-class systems problems, and provides a reproducible foundation for designing the scheduling, reconstruction, and variance-aware execution strategies needed to make cutting practical at scale. In addition to the future directions discussed previously, we will explore the integration of our *DistributedEstimator* in quantum application deployment and management frameworks such as QFaaS [48].

## 8. CRediT Authorship Contribution Statement

**Prabhjot Singh:** Conceptualization, Methodology, Software, Investigation, Data curation, Formal analysis, Visualization, Writing – original draft. **Adel N. Toosi:** Conceptualization, Supervision, Writing – review & editing. **Rajkumar Buyya:** Conceptualization, Supervision, Idea refinement, Scope definition, Understanding evaluation metrics, Writing – review & editing.

## References

- [1] J. Preskill, Quantum computing in the NISQ era and beyond, *Quantum* 2 (2018) 79. doi:10.22331/q-2018-08-06-79.
- [2] M. Cerezo, A. Arrasmith, R. Babbush, S. C. Benjamin, S. Endo, K. Fujii, J. R. McClean, K. Mitarai, X. Yuan, L. Cincio, P. J. Coles, Variational quantum algorithms, *Nature Reviews Physics* 3 (9) (2021) 625–644. doi:10.1038/s42254-021-00348-9.
- [3] S. Endo, Z. Cai, S. C. Benjamin, X. Yuan, Hybrid quantum-classical algorithms and quantum error mitigation, *Journal of the Physical Society of Japan* 90 (3) (2021) 032001. doi:10.7566/JPSJ.90.032001.
- [4] M. Schuld, V. Bergholm, C. Gogolin, J. Izaac, N. Killoran, Evaluating analytic gradients on quantum hardware, *Physical Review A* 99 (3) (2019) 032331. doi:10.1103/PhysRevA.99.032331.
- [5] K. Temme, S. Bravyi, J. M. Gambetta, Error mitigation for short-depth quantum circuits, *Physical Review Letters* 119 (18) (2017) 180509. doi:10.1103/PhysRevLett.119.180509.
- [6] J. Dean, S. Ghemawat, MapReduce: Simplified data processing on large clusters, in: *Proceedings of the 6th USENIX Symposium on Operating Systems Design and Implementation (OSDI)*, 2004, pp. 137–150. URL <https://research.google.com/archive/mapreduce-osdi04.pdf>
- [7] M. Zaharia, A. Konwinski, A. D. Joseph, R. Katz, I. Stoica, Improving MapReduce performance in heterogeneous environments, in: *Proceedings of the 8th USENIX Symposium on Operating Systems Design and Implementation (OSDI)*, 2008. URL [https://www.usenix.org/event/osdi08/tech/full\\_papers/zaharia/](https://www.usenix.org/event/osdi08/tech/full_papers/zaharia/)
- [8] A. Sergeev, M. Del Balso, Horovod: fast and easy distributed deep learning in TensorFlow, arXiv preprint arXiv:1802.05799 (2018). doi:10.48550/arXiv.1802.05799.
- [9] T. Peng, A. W. Harrow, M. Ozols, X. Wu, Simulating large quantum circuits on a small quantum computer, *Physical Review Letters* 125 (15) (2020) 150504. doi:10.1103/PhysRevLett.125.150504.
- [10] W. Tang, T. Tomesh, M. Suchara, J. Larson, M. Martonosi, CutQC: Using small quantum computers for large quantum circuit evaluations, in: *Proceedings of the 26th ACM International Conference on Architectural Support for Programming Languages and Operating Systems (ASPLOS)*, 2021, pp. 473–486. doi:10.1145/3445814.3446758.
- [11] C. Piveteau, D. Sutter, Circuit knitting with classical communication, *IEEE Transactions on Information Theory* 70 (5) (2024) 3001–3016, preprint: arXiv:2205.00016. doi:10.1109/TIT.2023.3310797.
- [12] A. W. Harrow, A. Lowe, Optimal quantum circuit cuts with application to clustered Hamiltonian simulation, *PRX Quantum* 6 (1) (2025) 010316. doi:10.1103/PRXQuantum.6.010316.
- [13] A. Lowe, M. Medvidović, A. Hayes, L. J. Romero, N. M. Tubman, D. Camps, Fast quantum circuit

- cutting with randomized measurements, *Quantum* 7 (2023) 934. doi:10.22331/q-2023-03-02-934.
- [14] A. Madry, A. Makelov, L. Schmidt, D. Tsipras, A. Vladu, Towards deep learning models resistant to adversarial attacks, in: *International Conference on Learning Representations (ICLR)*, 2018. URL <https://openreview.net/forum?id=rJzIBfZAb>
- [15] F. Tramèr, A. Kurakin, N. Papernot, I. Goodfellow, D. Boneh, P. McDaniel, Ensemble adversarial training: Attacks and defenses, in: *International Conference on Learning Representations (ICLR)*, 2018. URL <https://openreview.net/forum?id=rkZvSe-RZ>
- [16] P. Moritz, R. Nishihara, S. Wang, A. Tumanov, R. Liaw, E. Liang, M. Elibol, Z. Yang, W. Paul, M. I. Jordan, I. Stoica, Ray: A distributed framework for emerging AI applications, in: *Proceedings of the 13th USENIX Symposium on Operating Systems Design and Implementation (OSDI)*, 2018. URL <https://www.usenix.org/system/files/osdi18-moritz.pdf>
- [17] Qiskit Machine Learning Contributors, Qiskit machine learning, <https://qiskit.org/ecosystem/machine-learning/>, accessed: 2026-04 (2024).
- [18] Qiskit Addon Cutting Contributors, Circuit cutting with Qiskit addons, <https://qiskit.github.io/qiskit-addon-cutting/>, accessed: 2026-04 (2024).
- [19] A. Peruzzo, J. McClean, P. Shadbolt, M.-H. Yung, X.-Q. Zhou, P. J. Love, A. Aspuru-Guzik, J. L. O'Brien, A variational eigenvalue solver on a photonic quantum processor, *Nature Communications* 5 (2014) 4213. doi:10.1038/ncomms5213.
- [20] N. Moll, P. Barkoutsos, L. S. Bishop, J. M. Chow, A. Cross, D. J. Egger, S. Filipp, A. Fuhrer, J. M. Gambetta, M. Ganzhorn, A. Kandala, et al., Quantum optimization using variational algorithms on near-term quantum devices, *Quantum Science and Technology* 3 (3) (2018) 030503. doi:10.1088/2058-9565/aab822.
- [21] A. Kandala, A. Mezzacapo, K. Temme, M. Takita, M. Brink, J. M. Chow, J. M. Gambetta, Hardware-efficient variational quantum eigensolver for small molecules and quantum magnets, *Nature* 549 (7671) (2017) 242–246. doi:10.1038/nature23879.
- [22] J. Biamonte, P. Wittek, N. Pancotti, P. Rebentrost, N. Wiebe, S. Lloyd, Quantum machine learning, *Nature* 549 (7671) (2017) 195–202. doi:10.1038/nature23474.
- [23] K. Mitarai, M. Negoro, M. Kitagawa, K. Fujii, Quantum circuit learning, *Physical Review A* 98 (3) (2018) 032309. doi:10.1103/PhysRevA.98.032309.
- [24] V. Havlíček, A. D. Córcoles, K. Temme, A. W. Harrow, A. Kandala, J. M. Chow, J. M. Gambetta, Supervised learning with quantum-enhanced feature spaces, *Nature* 567 (7747) (2019) 209–212. doi:10.1038/s41586-019-0980-2.
- [25] H.-Y. Huang, M. Broughton, M. Mohseni, R. Babbush, S. Boixo, H. Neven, J. R. McClean, Power of data in quantum machine learning, *Nature Communications* 12 (2021) 2631. doi:10.1038/s41467-021-22539-9.
- [26] J. R. McClean, S. Boixo, V. N. Smelyanskiy, R. Babbush, H. Neven, Barren plateaus in quantum neural network training landscapes, *Nature Communications* 9 (2018) 4812. doi:10.1038/s41467-018-07090-4.
- [27] A. Javadi-Abhari, M. Treinish, K. Krsulich, C. J. Wood, J. Lishman, J. Gacon, S. Martiel, P. D. Nation, L. S. Bishop, A. W. Cross, B. R. Johnson, J. M. Gambetta, Quantum computing with Qiskit, arXiv preprint arXiv:2405.08810 (2024). doi:10.48550/arXiv.2405.08810.
- [28] IBM Quantum, Qiskit primitives API documentation (Estimator and Sampler), Online documentation, accessed: 2026-04 (2024). URL <https://quantum.cloud.ibm.com/docs/api/qiskit/primitives>
- [29] V. Bergholm, J. Izaac, M. Schuld, C. Gogolin, N. Killoran, et al., PennyLane: Automatic differentiation of hybrid quantum-classical computations, arXiv preprint arXiv:1811.04968 (2018). doi:10.48550/arXiv.1811.04968.

- [30] M. Broughton, G. Verdon, T. McCourt, A. J. Martinez, J. H. Yoo, S. V. Isakov, P. Massey, R. Halavati, M. Y. Niu, A. Zlokapa, et al., TensorFlow Quantum: A software framework for quantum machine learning, arXiv preprint arXiv:2003.02989 (2020). doi:10.48550/arXiv.2003.02989.
- [31] M. Zaharia, M. Chowdhury, T. Das, A. Dave, J. Ma, M. McCauley, M. J. Franklin, S. Shenker, I. Stoica, Resilient distributed datasets: A fault-tolerant abstraction for in-memory cluster computing, in: Proceedings of the 9th USENIX Symposium on Networked Systems Design and Implementation (NSDI), 2012. URL <https://www.usenix.org/conference/nsdi12/>
- [32] M. Rocklin, Dask: Parallel computation with blocked algorithms and task scheduling, in: Proceedings of the 14th Python in Science Conference (SciPy), 2015, pp. 126–132. doi:10.25080/Majora-7b98e3ed-013.
- [33] M. Li, D. G. Andersen, J. W. Park, A. J. Smola, A. Ahmed, V. Josifovski, J. Long, E. J. Shekita, B.-Y. Su, Scaling distributed machine learning with the parameter server, in: Proceedings of the 12th USENIX Symposium on Operating Systems Design and Implementation (OSDI), 2014, pp. 583–598. URL <https://www.usenix.org/conference/osdi14/>
- [34] Q. Ho, J. Cipar, H. Cui, J. K. Kim, S. Lee, P. B. Gibbons, G. Gibson, G. R. Ganger, E. P. Xing, More effective distributed ML via a stale synchronous parallel parameter server, in: Advances in Neural Information Processing Systems (NeurIPS), 2013. URL <https://papers.neurips.cc/paper/4894>
- [35] B. Recht, C. Re, S. Wright, F. Niu, Hogwild!: A lock-free approach to parallelizing stochastic gradient descent, in: Advances in Neural Information Processing Systems (NeurIPS), 2011. URL <https://proceedings.neurips.cc/paper/2011/hash/218a0aefd1d1a4be65601cc6ddc1520e>
- [36] M. Cho, et al., BlueConnect: Decomposing all-reduce for deep learning on heterogeneous network hierarchy, in: Proceedings of Machine Learning and Systems (MLSys), 2019. URL <https://mlsys.org/Conferences/2019/doc/2019/130.pdf>
- [37] P. Goyal, P. Dollár, R. B. Girshick, P. Noordhuis, L. Wesolowski, A. Kyrola, A. Tulloch, Y. Jia, K. He, Accurate, large mini-batch SGD: Training ImageNet in 1 hour, arXiv preprint arXiv:1706.02677 (2017). doi:10.48550/arXiv.1706.02677.
- [38] R. D. Blumofe, C. E. Leiserson, Scheduling multithreaded computations by work stealing, Journal of the ACM 46 (5) (1999) 720–748. doi:10.1145/324133.324234.
- [39] A. Carrera Vazquez, C. Tornow, D. Ristè, S. Wornner, M. Takita, D. J. Egger, Combining quantum processors with real-time classical communication, Nature 636 (2024) 75–79. doi:10.1038/s41586-024-08178-2.
- [40] J. Garrison, et al., Circuit cutting with Quantum Serverless, IBM Research, accessed: 2026-04 (2023). URL <https://research.ibm.com/publications/circuit-cutting-with-quantum-serverless>
- [41] I. Sitdikov, et al., Circuit knitting toolbox and quantum serverless, IBM Research, accessed: 2026-04 (2023). URL <https://research.ibm.com/publications/circuit-knitting-toolbox-and-quantum-serverless>
- [42] C. Johnson, et al., Simulating larger quantum circuits with circuit cutting and Quantum Serverless, SC 2023 Poster, IBM Research, accessed: 2026-04 (2023). URL <https://research.ibm.com/publications/simulating-larger-quantum-circuits-with-circuit-cutting-and-quantum-serverless>
- [43] C. Szegedy, W. Zaremba, I. Sutskever, J. Bruna, D. Erhan, I. Goodfellow, R. Fergus, Intriguing properties of neural networks, arXiv preprint arXiv:1312.6199 (2013). doi:10.48550/arXiv.1312.6199.
- [44] I. J. Goodfellow, J. Shlens, C. Szegedy, Explaining and harnessing adversarial examples, in: International Conference on Learning Representations

- (ICLR), 2015.  
URL <https://arxiv.org/abs/1412.6572>
- [45] Qiskit Contributors, Qiskit: An open-source framework for quantum computing, <https://qiskit.org>, accessed: 2026-04 (2024).
- [46] Y. LeCun, L. Bottou, Y. Bengio, P. Haffner, Gradient-based learning applied to document recognition, *Proceedings of the IEEE* 86 (11) (1998) 2278–2324. doi:10.1109/5.726791.
- [47] R. A. Fisher, The use of multiple measurements in taxonomic problems, *Annals of Eugenics* 7 (2) (1936) 179–188. doi:10.1111/j.1469-1809.1936.tb02137.x.
- [48] H. T. Nguyen, M. Usman, R. Buyya, Qfaas: A serverless function-as-a-service framework for quantum computing, *Future Generation Computer Systems* 154 (2024) 281–300. doi:<https://doi.org/10.1016/j.future.2024.01.018>.  
URL <https://www.sciencedirect.com/science/article/pii/S0167739X24000189>